Synchronization of Two Microwave Sources With Femtosecond-level Residual Timing Jitters Using a Microwave Photonic Phase Detector

Kunlin Shao, Yamei Zhang, *Member, IEEE*, Penghui Gao, Feng Yang, Jianing Zhao, Shuo Liu, Ping Li, Xiaohu Tang, Zhongyang Xu, *Member, IEEE*, and Shilong Pan, *Senior Member, IEEE, Fellow, OPTICA*

***Abstract*—A microwave photonic phase detector (MPPD) for simultaneous synchronization of two independent microwave sources to a single mode-locked laser (MLL) with femtosecond-level residual timing jitters is firstly proposed and experimentally demonstrated. A Sagnac loop is built based on a dual-polarization dual-drive Mach-Zehnder modulator (DP-DMZM). Each path consisting a branch of the modulator forms an MPPD due to its feature of polarization multiplexing. Thus, two dielectric resonator oscillators (DROs) can be synchronized simultanesously. A proof-of-concept experiment is carried out. Two independent DROs with frequencies of 8.0320 and 8.3332 GHz are synchronized to an MLL. The phase noises of the synchronized 8.0320-GHz signal are -109.79 and -135.14 dBc/Hz at the 1-kHz and 10-kHz offset frequencies, respectively, and those of the 8.3332-GHz signal are -106.87 and -133.86 dBc/Hz. The residual timing jitters of the two synchronized signals (integrated from 100 Hz to 1 MHz) are around 2.12 fs and 5.93 fs, respectively. The impact of the amplitude and phase imbalances of the driven signals to the DP-DMZM on the performance of the MPPD is investigated.**

***Index Terms*—Microwave photonic phase detector, femtosecond pulse, synchronization, photonic locking loop.**

I. INTRODUCTION

Synchronization of multiple microwave signals is of great importance for sampling systems, distributed radars, quantum science, and so on [1]–[3], which is generally realized through synchronizing multiple microwave signals to a specific reference signal with a phase-locked loop [4]–[5]. Traditionally, the reference signal and the phase-locked loop are obtained using pure electronic circuits, which, however, suffer seriously from low-frequency, poor phase detection sensitivity, and high noise floor. Thanks to the low timing jitter and ultra-low phase noise provided by the mode-locking technique [6]–[7], a mode-locked laser (MLL) is widely used as the reference signal in a synchronization system [8]–[13]. The key to the MLL-based synchronization system is to realize a microwave photonic phase detector (MPPD). Compared with the electronic phase detector, the MPPD shows outstanding performance associated with large operation bandwidth, high phase detection sensitivity, and low noise floor, which has attracted much attention.

The basic principle of an MPPD is to sample a microwave signal with an optical pulse train. When the frequency of the microwave signal is N (N is an integer) times the repetitive frequency of the optical pulse, the pulse would locate at the same position of the microwave signal in each period. Therefore, after a low-speed photodetector (PD), the phase error between the optical pulse and the microwave signal would be mapping to the output voltage of the PD. An MPPD can thus be realized. However, with a single channel, the common-mode noise cannot be eliminated, which would worsen the noise floor of the MPPD. To deal with this, two channels with a phase bias between them can be built. Applying the two channels to a balanced PD (BPD), the common-mode noise can be eliminated, and an MPPD with a low residual noise floor can be obtained.

A Sagnac loop is often established to achieve the MPPD with balanced photodetection. The Sagnac-loop-based MPPD is generally realized with an MLL, an optical coupler, a uni-traveling phase modulator (PM), a phase bias device, and a BPD. An optical pulse train is generated by the MLL and is coupled into the Sagnac loop composed of the 2×2 optical coupler, the PM, and the phase bias device. In the loop, the copropagating pulse train experiences phase modulation while the counter-propagating wave does not due to the uni-traveling property of the PM. Then the two waves interfere with each other at the two outputs of the Sagnac loop, where phase modulation to amplitude modulation conversion is performed. When there is a phase bias between the two counter-propagating pulse trains, the two outputs of the Sagnac loop would experience different amplitude modulations. After balanced photodetection, an electrical signal with its voltage proportional to the phase error between the optical pulse and the electrical driven signal can be generated, which can be fed back to realize the synchronization. As a result, the microwave signal can be synchronized to the MLL. The first Sagnac-loop-based MPPD was proposed by J. Kim *et al.* [9] in 2004, in which a spatial structure and a $\pi/2$ phase bias device was employed. This work is pioneering, and the lowest residual noise of the work is around -130 dBc/Hz. However, the spatial structure makes the system bulky, complex and susceptive to environmental vibrations. To deal with this problem, a fiber-

Manuscript received xx xx, xxxx; revised xx xx, xxxx and xx xx, xxxx; accepted xx xx, xxxx. Date of publication xx xx, xxxx; date of current version xx xx, xxxx. This work was supported in part by the National Natural Science Foundation of China under Grant (61901215, 62171219), and in part by the Jiangsu Natural Science Foundation under Grant BK20190404. (*Corresponding author: Yamei Zhang; Shilong Pan*).

The authors are with the Key Laboratory of Radar Imaging and Microwave Photonics (Nanjing Univ. Aeronaut. Astronaut.), Ministry of Education, Nanjing University of Aeronautics and Astronautics, Nanjing 210016, China (e-mail: zhang_ym@nuaa.edu.cn; pans@nuaa.edu.cn).

Color versions of one or more of the figures in this article are available online at http://ieeexplore.ieee.org

Digital Object Identifier xxxxxx.

based Sagnac loop was reported [14]. The residual phase noise was significantly decreased to -133 dBc/Hz and -154 dBc/Hz at 1-Hz and 5-kHz offset frequency, respectively. But the π/2 phase bias is realized by two Faraday rotators (FRs) and a quarter-wave plate, which is also complex and sensitive to vibrations and temperature variation. To avoid the use of the π/2 phase-shifted device, a 3×3 optical coupler was used to build a Sagnac loop [15]. In the 3×3 optical coupler, there is an inherent 2π/3 phase difference between adjacent outputs, which introduces a 2π/3 phase bias to the two counter-propagating pulse trains of the Sagnac loop. The minimum residual phase noise floor of this work reaches < -154 dBc/Hz (at 8-GHz carrier frequency) with an integrated root mean square (RMS) timing jitter of 0.97 fs [1 Hz–1 MHz]. The Sagnac-loop-based MPPD is simple and easy to operate which has been widely studied.

In addition to the Sagnac-loop-based MPPD, MPPDs with a straightforward structure are also reported and investigated [16]–[19]. It can be realized by a dual-output Mach-Zehnder modulator (DOMZM) [16]–[17], a polarization modulator (PolM) [18], or a dual-polarization dual-drive Mach-Zehnder modulator (DP-DMZM) [19].

However, all the previously reported MPPDs can only synchronize a single microwave signal to an MLL. In some applications, such as measurement systems and distributed systems, multiple synchronized microwave sources are required.

In this paper, an MPPD that can detect the phase errors between two independent microwave sources and one single MLL, respectively, is proposed and experimentally demonstrated based on the polarization-division multiplexing technique. The two phase errors are then fed back to the two independent microwave sources, and the two microwave sources can be synchronized to the MLL simultaneously. An experiment is carried out. Two dielectric resonator oscillators (DROs) with frequencies of 8.0320 GHz and 8.3332 GHz are locked to a single MLL with a repetition rate of 100.4 MHz. The residual noises between the two RF signals and the harmonics of the MLL are much lower than the absolute phase noise at offset frequencies below 10 kHz, indicating that the phase noises of the microwaves follow that of the MLL. The locked microwaves have phase noises of -135.14 dBc/Hz and -133.86 dBc/Hz at the offset frequency of 10 kHz, and the integrated residual timing jitters are around 2.12 fs and 5.93 fs, respectively. The phase coherence of the two microwaves is evaluated, the independence of the phase detection of the two microwaves is discussed, and the influence of the amplitude and phase imbalances of the RF driven signal of the DP-DMZM is investigated.

II. Principle and Analysis

Fig. 1(a) shows the schematic diagram of the proposed MPPD, which is consisted of an MLL, a Sagnac loop, two DROs, two electrical power dividers, two polarization beam splitters (PBSs), and two BPDs. The MLL emits an optical pulse train with an ultra-narrow pulse width at the order of

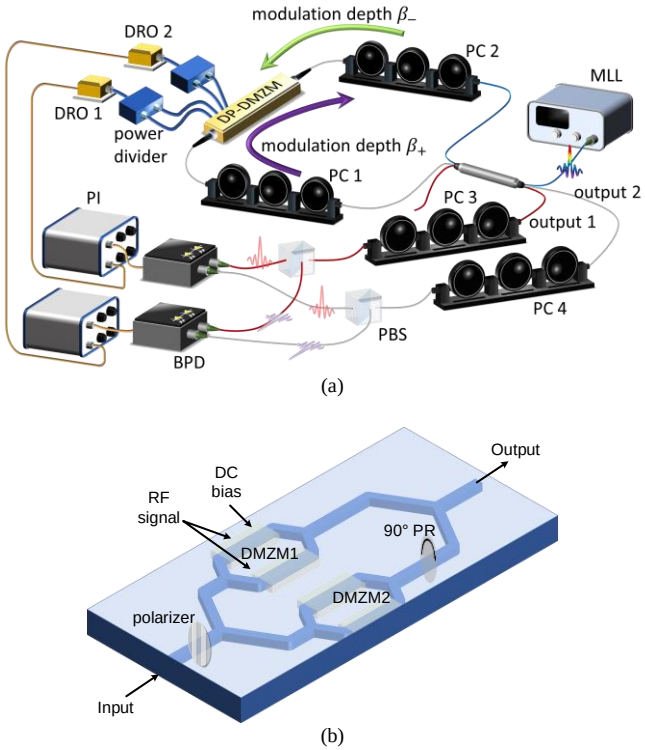

Fig. 1. (a) Schematic diagram of the proposed MPPD. MLL: mode-locked laser; DP-DMZM: dual-polarization dual-drive Mach-Zehnder modulator; PC: polarization controller; PBS: polarization beam splitter; BPD: balanced photodetector; DRO: dielectric resonator oscillator; PI: proportional-integral controller. (b) Inner structure of the DP-DMZM. DMZM: dual-drive Mach-Zehnder modulator; PR: polarization rotator.

magnitude of femtosecond. Since the period of the microwave signal is about several hundred picoseconds, the pulse train can be expressed as an impulse function approximately,

$$E_{\text{pulse}}(t) = A\sum_{n=0}^{\infty}\delta\left(t-\frac{n}{f_{\text{rep}}}\right) \tag{1}$$

where A is the amplitude of each pulse, and f_{rep} is the repetition rate of the MLL. Here, the amplitude fluctuation and the period timing jitter are neglected, i.e., A and f_{rep} are considered constant.

The optical pulse train is then coupled into the Sagnac loop consisting of a 3×3 coupler, a DP-DMZM, and two polarization controllers (PCs). The DP-DMZM is an integrated modulator comprises a polarizer, a 3-dB optical coupler, two sub-DMZMs, a 90-degree polarization rotator (PR), and a power combiner, which has two optical ports, four RF input ports, and two DC bias ports, as shown in Fig. 1(b). When two identical RF signals are applied to one sub-DMZM, phase modulation is achieved. When the optical pulse train is transmitted from optical port1 to optical port2, the output signal would have two orthogonal state-of-polarizations (SOPs) due to the existence of the PR. When the light is transmitted from optical port2 to optical port1, the output signal would have only one SOP owing to the existence of the polarizer. In addition, since the DP-DMZM is a non-reciprocal device, the modulation index of the DP-DMZM is different when the light propagates along different directions. As shown in Fig. 1(a), the modulation index is β_+ when light propagates in the loop and is β_- when light counter

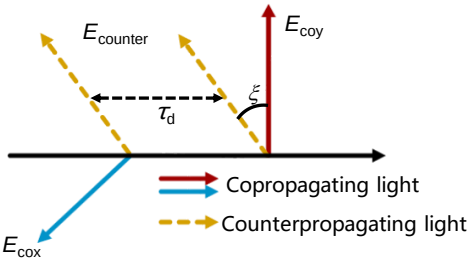

Fig. 2. The optical field at the output of the 3×3 optical coupler when there is a delay difference between upper and lower branch of the DP-DMZM.

propagates in the loop, and $\beta_+ > \beta_-$. The two optical pulse trains from different directions will interfere at the outputs of the Sagnac loop, converting the phase modulation to amplitude modulation.

Mathematically, supposing the expressions of the microwaves generated by the DROs are,

$$m_i(t) = a_i \sin(2\pi f_i t + \varphi_i) \quad (i = 1, 2) \tag{2}$$

where a_i is the amplitude, f_i is the frequency, and φ_i is the phase error between the microwave and the optical pulse. It is demanded that f_i should be equal to $N \cdot f_{rep}$ (N is an integer).

The transmission matrix of the 3×3 optical coupler is given in [20], shown below,

$$M = \frac{1}{\sqrt{3}} \begin{bmatrix} 1 & 1 & 1 \\ 1 & e^{j\frac{2\pi}{3}} & e^{-j\frac{2\pi}{3}} \\ 1 & e^{-j\frac{2\pi}{3}} & e^{j\frac{2\pi}{3}} \end{bmatrix} \tag{3}$$

Thus, the signal at output1 of the Sagnac loop can be written as,

$$\begin{bmatrix} E_{cox1} \\ E_{coy1} \end{bmatrix} \propto \begin{bmatrix} E_{pulse}(t) e^{j\beta_{1+}\sin\varphi_1} \\ E_{pulse}(t-\tau_d) e^{j\beta_{2+}\sin\varphi_2} \end{bmatrix} \tag{4}$$

$$\begin{aligned} E_{counter1} \propto & \cos\xi \cdot E_{pulse}(t) e^{j\beta_{1-}\sin\varphi_1 + j\frac{4\pi}{3}} \\ & + \sin\xi \cdot E_{pulse}(t-\tau_d) e^{j\beta_{2-}\sin\varphi_2 + j\frac{4\pi}{3}} \end{aligned} \tag{5}$$

where E_{cox1} and E_{coy1} represent the copropagating pulses along the two orthogonal polarization directions, respectively, $E_{counter1}$ represents the counterclockwise propagating pulse, β_{1+} and β_{2+} are the modulation indices of the upper branch and lower branch along the clockwise propagation direction, respectively, β_{1-} and β_{2-} represent modulation indices of the upper and lower branch along the counterclockwise propagation direction, τ_d is the time difference between the two branches of the DP-DMZM, which is around several picoseconds according to the datasheet of the DP-DMZM, and ξ is the angle between the principal axes of the polarizer in the modulator and the polarization direction of the counterclockwise propagating lightwave. The illustration of the signal at output1 of the Sagnac loop is displayed in Fig. 2, where the red and blue lines represent the copropagating pulse trains and the yellow dashed line represents the counter-propagating pulse trains. Due to the time delay between the two main principal axes of the DP-DMZM, the pulse trains along the two branches are separated in the time domain when arriving at the loop output.

Then the signal in Fig. 2 is applied to a PC (PC3) and a PBS (PBS1). The principal axes of the PBS are aligned to be the same as the principal axes of the DP-DMZM. Therefore, the output of PBS1 can be written as,

$$\begin{bmatrix} E_{X1} \\ E_{Y1} \end{bmatrix} \propto \begin{bmatrix} E_{cox1} + \cos\gamma \cdot E_{counter1} \\ E_{coy1} + \sin\gamma \cdot E_{counter1} \end{bmatrix} \tag{6}$$

where γ is the angle between the principal axes of the PBS and the polarization direction of $E_{counter1}$.

Similarly, the signal at ouput2 of the 3×3 optical coupler can be expressed as

$$\begin{bmatrix} E_{cox2} \\ E_{coy2} \end{bmatrix} \propto \begin{bmatrix} E_{pulse}(t) e^{j\beta_{1+}\sin\varphi_1 - j\frac{2\pi}{3}} \\ E_{pulse}(t-\tau_d) e^{j\beta_{2+}\sin\varphi_2 - j\frac{2\pi}{3}} \end{bmatrix} \tag{7}$$

$$\begin{aligned} E_{counter2} \propto & \cos\xi \cdot E_{pulse}(t) e^{j\beta_{1-}\sin\varphi_1} \\ & + \sin\xi \cdot E_{pulse}(t-\tau_d) e^{j\beta_{2-}\sin\varphi_2} \end{aligned} \tag{8}$$

And the signal at the output of PBS2 is,

$$\begin{bmatrix} E_{X2} \\ E_{Y2} \end{bmatrix} \propto \begin{bmatrix} E_{cox2} + \cos\gamma \cdot E_{counter2} \\ E_{coy2} + \sin\gamma \cdot E_{counter2} \end{bmatrix} \tag{9}$$

Then two output signals along the x-polarization direction are applied to the two optical input ports of a BPD (BPD1), respectively, and those along the y-polarization direction are applied to the two optical input ports of another BPD (BPD2), respectively. The response speed of the BPD is low, so only the average optical power difference is detected. The output of each BPD is shown as follows,

$$\begin{aligned} \Delta P_x &= |E_{X1}|^2 - |E_{X2}|^2 \\ &\propto \sqrt{3}\,\Re G \cos\gamma \cos\xi \sin[(\beta_{1+} - \beta_{1-})\sin\varphi_1] \\ &\approx \sqrt{3}\,\Re G \cos\gamma \cos\xi \cdot (\beta_{1+} - \beta_{1-})\varphi_1 \end{aligned} \tag{10}$$

$$\begin{aligned} \Delta P_y &= |E_{Y1}|^2 - |E_{Y2}|^2 \\ &\propto \sqrt{3}\,\Re G \sin\gamma \cos\xi \sin[(\beta_{2+} - \beta_{2-})\sin\varphi_2] \\ &\approx \sqrt{3}\,\Re G \sin\gamma \cos\xi \cdot (\beta_{2+} - \beta_{2-})\varphi_2 \end{aligned} \tag{11}$$

where $\Re$ is the responsivity of the BPD, and G is the trans-impedance gain of the BPD. It can be seen from Eq. (10) and Eq. (11), φ_1 and φ_2 can be extracted independently as they are proportional to the output voltages of the BPD. The detection sensitivity depends mainly on the difference between the copropagating and counter-propagating modulation indices and the SOP of the counter-propagating signal at the output ports of the Sagnac loop.

III. Experimental Results

An experiment is established according to the setup shown in Fig. 1(a) to prove the feasibility of the proposed scheme. An MLL (Menlo, C-Fiber) with a repetition rate of 100.4 MHz is employed to generate the optical pulse train with a pulse width less than 90 fs, and the average output optical power is about 20 dBm. The pulse train is then injected into the Sagnac loop consisting of two PCs (PC1 and PC2), a 20-GHz DP-DMZM (Fujitsu, FTM 7980), and a 3×3 optical coupler. The two PCs

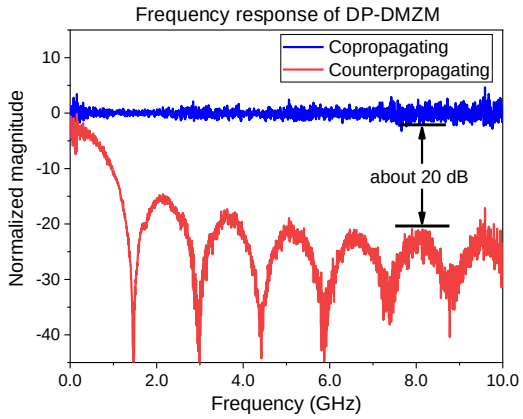

Fig. 3. Frequency responses of the DP-DMZM under copropagating and counterpropagating modulation.

are placed before and after the DP-DMZM, respectively, to guarantee the SOP of the optical pulse. The DP-DMZM is driven by two microwave signals that are generated by two DROs (DRO1 and DRO2). DRO1 (HMC-C200 8000) generates an 8.0320-GHz microwave signal with a power of 13 dBm, and DRO2 (WTDRO-08300-10) generates an 8.3332-GHz microwave signal with a power of 12 dBm. To improve the locking performance, the two signals are then amplified to more than 20 dBm. To achieve the phase modulation for each sub-DMZM, the driven microwave signal is split into two paths by a power divider before being applied to the DP-DMZM. Two BPDs (THORLABS PDB450C) with a bandwidth of 50 MHz and responsivity of 1 A/W are employed to perform the optical to electrical conversion. A PI controller captures the output signal of each BPD to produce a control signal which is then fed back to the DRO to compensate for the phase error. As a result, the two DROs are synchronized to the MLL.

Firstly, the non-reciprocal property of the DP-DMZM is evaluated since it is the foundation of the proposed MPPD. A vector network analyzer (VNA, Rohde & Schwarz, ZVA 67) is employed to measure the frequency response of the DP-DMZM, and the measured frequency responses are shown in Fig. 3. In Fig. 3, the blue curve is the frequency response when the lightwave is copropagating in the DP-DMZM while the red curve is the frequency response when the lightwave is counter-propagating in the DP-DMZM. The curves are normalized by the copropagating response. It can be seen that the two frequency responses are extremely different, indicating that the DP-DMZM is exactly a non-reciprocal device. Moreover, in the interested frequency range, i.e., around 8 GHz (according to the frequency of the DROs), there is about a 20-dB magnitude response difference, which is enough for the reliability of the proposed MPPD.

Then the electrical spectra of the two microwave signals before and after being synchronized to the MLL are observed, as shown in Fig. 4. The blue curves are the spectra before being locked, and the red curves are the spectra after being locked. The zoom-in version of the spectra around DRO1 and DRO2 are displayed in Fig. 4 (b) and Fig. 4 (c), respectively. The several spurs in Fig. 4(c) is caused by the amplifier we use. By

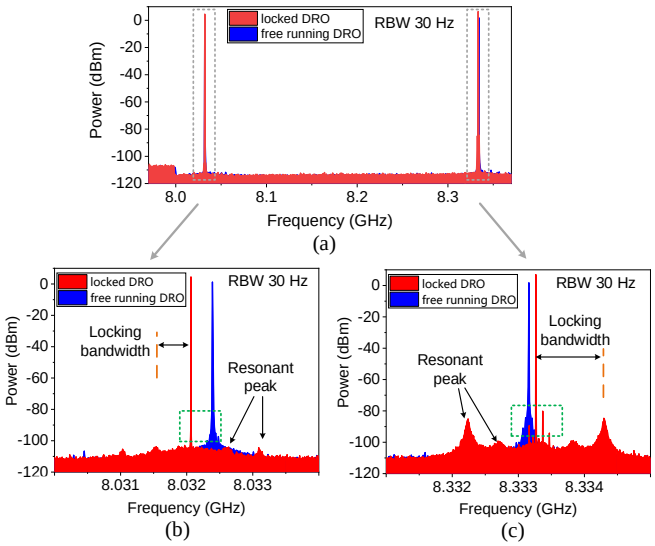

Fig. 4. (a) Spectrum of the two microwaves before and after being locked. (b) Spectrum of the 8.0320-GHz microwave before and after being locked. (c) Spectrum of the 8.3332-GHz microwave before and after being locked.

comparing the spectra in the green dashed box, the linewidths of the locked signals are obviously narrower than that of the unlocked signals at low offset frequency, indicating that the two microwave sources are successfully locked to the MLL simultaneously. It should be noted that, there are two pairs of symmetrical resonant peaks observed in each locked curve, which are mainly resulted by the locking bandwidth of the system and can be weakened by adding a lead compensator [18]. The difference between the two locking bandwidths is mainly due to the different detection sensitivities and different tuning sensitivities of the DROs.

The phase noises of the two DROs before and after being locked to the MLL are depicted in Fig. 5 with the blue curves and the red curves. The values of phase noises at some typical offset frequencies are listed in Table I. As can be seen, the phase noise of the 8.0320-GHz signal reduces from -61.89 dBc/Hz to -109.79 dBc/Hz at 1-kHz offset frequency, and from -84.72 dBc/Hz to -135.14 dBc/Hz at 10-kHz offset frequency.

TABLE I
PHASE NOISE AT TYPICAL OFFSET FREQUENCIES

8.0320-GHz

Offset frequency	Phase noise (unlocked) (dBc/Hz)	Phase noise (locked) (dBc/Hz)
1 Hz	22.55	-26.06
100 Hz	-35.71	-89.59
1 kHz	-61.89	-109.79
10 kHz	-84.72	-135.14
100 kHz	-119.39	-147.39

8.3332-GHz

Offset frequency	Phase noise (unlocked) (dBc/Hz)	Phase noise (locked) (dBc/Hz)
1 Hz	6.93	-26.52
100 Hz	-45.67	-89.63
1 kHz	-72.02	-106.87
10 kHz	-95.91	-133.86
100 kHz	-117.03	-141.21

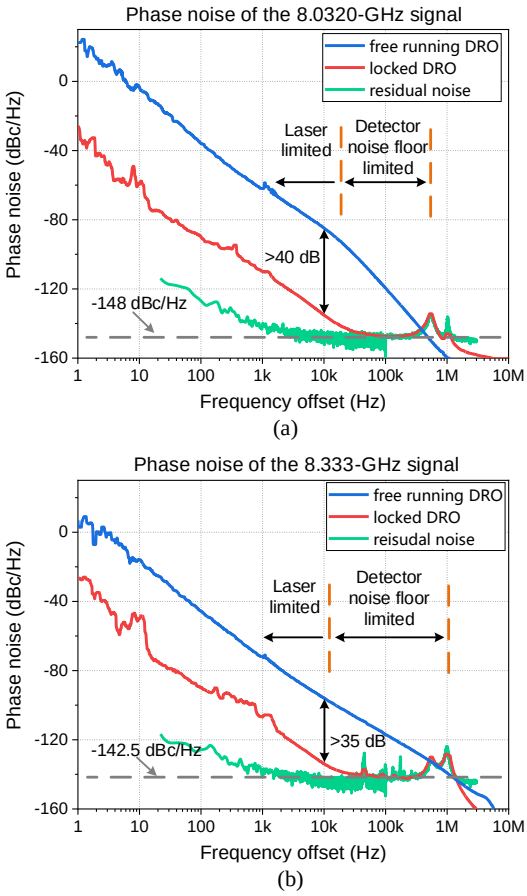

Fig. 5. (a) The phase noise of the 8.0320-GHz signal. (b) The phase noise of the 8.3332-GHz signal.

Correspondingly, the phase noise of the 8.3332-GHz signal reduces from -72.02 dBc/Hz to -106.87 dBc/Hz and from -95.91 dBc/Hz to -133.86 dBc/Hz at offset frequencies of 1 kHz and 10 kHz, respectively. The phase noise at 10 kHz offset frequency is improved by more than 40 dB (35 dB) for 8.0320-GHz (8.3332-GHz) signal.

The residual phase noises between the optical pulse and the microwave signals are also measured as shown as the green curves in Fig. 5, which are the phase noise difference between the two locked microwaves and the MLL, representing the noise floor of the MPPD. To do so, another single-tone MPPD based on a DP-DMZM [19] is built, as shown in Fig. 6, in which the two locked microwaves are sequentially injected into the single-tone phase detector, and the output of the single-tone phase detector would be the residual noise between the locked microwave and the optical pulse trains. The residual noise curves in Fig. 5(a) and Fig. 5(b) are lower than the phase noise of the locked microwave, indicating that the phase noises of the locked microwaves follow the phase noise of the MLL at low offset frequencies, while at high offset frequencies, it is dominated by the noise floor of the phase detector. The noise floor is around -140 dBc/Hz (-137 dBc/Hz) at the 1-kHz offset frequency, and the lowest noise floor is around -148 dBc/Hz (-142.5 dBc/Hz) for 8.0320-GHz (8.3332-GHz) signal. Since the DC component of the residual noise cannot be suppressed completely, the residual noise below 100 Hz is not that accurate.

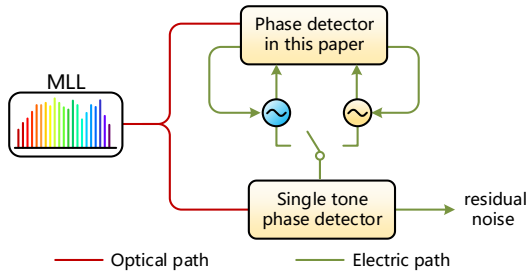

Fig. 6. The experimental setup for residual noise measurement.

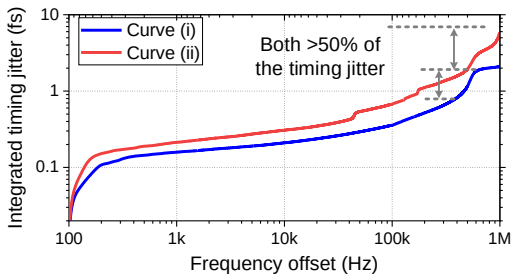

Fig.7. Integrated residual timing jitter of the two locked microwaves. Curve (i): jitter of the 8.0320-GHz signal. Curve (ii): jitter of the 8.3332-GHz signal.

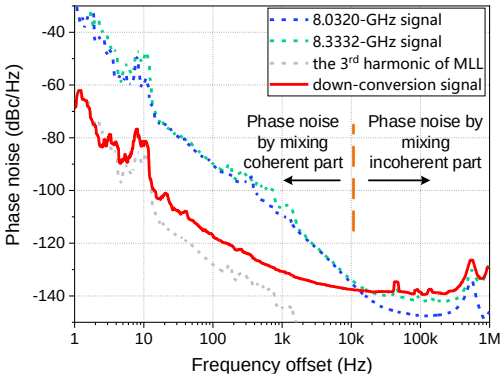

Fig. 8. Phase noise of the down-conversion microwave. The regimes with different colors represent different factors limited phase noise.

Therefore, the integrated residual timing jitters of the two locked DROs are calculated from 100 Hz to 1 MHz, as shown in Fig. 7. As can be seen, for DRO1 (DRO2), the residual integrated timing jitters are around 2.12 fs (5.93 fs), showing that the two DROs are synchronized at the same level. The curves also show that the resonant peaks contribute more than 50% of the timing jitter, and a lead compensator will reduce them dramatically.

In [21] and [22], residual noises below -160 dBc/Hz were achieved. The key component is a Mach-Zehnder interferometer (MZI)-based pulse repetition rate multiplier (PRRM). Since the two microwave frequencies chosen here do not have common divisor that is an integral multiple of 100.4 MHz, MZI-PRRM cannot be used here. But it is believed that MZI-PRRM can reduce the residual noise significantly if appropriate DRO frequencies are selected.

Then the two locked microwaves are mixed in a mixer to further approve that the two microwaves are synchronized to each other. Fig. 8 shows the measured phase noise of the

frequency down-conversion signal around 301 MHz (red line) compared to the phase noises of the synchronized microwaves. It is seen that the phase noise of the frequency down-converted signal follows the phase noise of the 3rd order harmonic below 10-Hz offset frequency, and is much lower than the phase noises of the two signals before mixing at offset frequencies smaller than 10 kHz, indicating that the two microwave signals are phase correlated at low-offset frequency. But the two microwaves become incoherent at high offset frequencies (larger than 10 kHz) as the phase noise of the frequency down-converted signal becomes even greater than the phase noises of the locked microwaves, which is mainly due to the noise floor of the phase detector and the other additional noise introduced during the mixing operation. This result shows that the two signals are synchronized to each other at a low offset frequencies.

IV. Discussion

A. No delay difference between the two branches of the DP-DMZM

Though there is often a time delay between the two branches of a DP-DMZM, we could not exclude the possibility that the time delay may be zero. So, the condition of none time delay between the two branches of the DP-DMZM is discussed. Through the discussion below, it can be found that there are some differences between these two cases.

As mentioned above, an optical signal with only one polarization state would be existing when the light transmits from optical port1 to optical port2 of the DP-DMZM. So, no time delay means the light counter-propagating in the two branches will interfere with each other. To solve this problem, PC2 should be adjusted to make ξ=0° in Eq. (5) and (8), under which case the counter-propagating pulse only carries the phase information of one microwave signal, and then the signal at output1 can be written as

$$\begin{bmatrix} E_{\mathrm{co}x1} \\ E_{\mathrm{co}y1} \end{bmatrix} \propto \begin{bmatrix} E_{\mathrm{pulse}}(t)e^{j\beta_{1+}\sin\varphi_1} \\ E_{\mathrm{pulse}}(t)e^{j\beta_{2+}\sin\varphi_2} \end{bmatrix} \tag{12}$$

$$E_{\mathrm{counter}1} \propto E_{\mathrm{pulse}}(t)e^{j\beta_{1-}\sin\varphi_1 + j\frac{4\pi}{3}} \tag{13}$$

The signal at output2 is given by

$$\begin{bmatrix} E_{\mathrm{co}x2} \\ E_{\mathrm{co}y2} \end{bmatrix} \propto \begin{bmatrix} E_{\mathrm{pulse}}(t)e^{j\beta_{1+}\sin\varphi_1 - j\frac{2\pi}{3}} \\ E_{\mathrm{pulse}}(t)e^{j\beta_{2+}\sin\varphi_2 - j\frac{2\pi}{3}} \end{bmatrix} \tag{14}$$

$$E_{\mathrm{counter}2} \propto E_{\mathrm{pulse}}(t)e^{j\beta_{1-}\sin(2\pi f_1 t+\varphi_1)} \tag{15}$$

The signals at the two outputs after the PBS can be respectively written as,

$$\begin{bmatrix} E_{\mathrm{X}1} \\ E_{\mathrm{Y}1} \end{bmatrix} \propto E_{\mathrm{pulse}}(t) \begin{bmatrix} e^{j\beta_{1+}\sin\varphi_1} + \cos\gamma \cdot e^{j\beta_{1-}\sin\varphi_1 + j\frac{4\pi}{3}} \\ e^{j\beta_{2+}\sin\varphi_2} + \sin\gamma \cdot e^{j\beta_{1-}\sin\varphi_1 + j\frac{4\pi}{3}} \end{bmatrix} \tag{16}$$

$$\begin{bmatrix} E_{\mathrm{X}2} \\ E_{\mathrm{Y}2} \end{bmatrix} \propto E_{\mathrm{pulse}}(t) \begin{bmatrix} e^{j\beta_{1+}\sin\varphi_1 - j\frac{2\pi}{3}} + \cos\gamma \cdot e^{j\beta_{1-}\sin\varphi_1} \\ e^{j\beta_{2+}\sin\varphi_2 - j\frac{2\pi}{3}} + \sin\gamma \cdot e^{j\beta_{1-}\sin\varphi_1} \end{bmatrix} \tag{17}$$

From Eq. (16) and Eq. (17), we can obtain that φ_1 and φ_2 cannot be separated in the optical domain. The power difference between $E_{\mathrm{X}1}$ and $E_{\mathrm{X}2}$ is calculated to be,

$$\begin{aligned} \Delta P_x &\propto \sqrt{3}\,\Re G\cos\gamma \cdot \sin[(\beta_{1+}-\beta_{1-})\sin\varphi_1] \\ &\approx \sqrt{3}\,\Re G\cos\gamma \cdot (\beta_{1+}-\beta_{1-})\varphi_1 \end{aligned} \tag{18}$$

The phase error φ_1 is proportional to the power difference of the BPD1, which can be extracted and compensated with a feedback loop. So the phase error φ_1 would become to 0 after phase error compensation. As φ_1 equals zero, the power difference between E_{Y1} and E_{Y2} can be detected as,

$$\begin{aligned} \Delta P_y &\propto \sqrt{3}\,\Re G\sin\gamma \cdot \sin[\beta_{2+}\sin\varphi_2] \\ &\approx \sqrt{3}\,\Re G\sin\gamma \cdot \beta_{2+}\varphi_2 \end{aligned} \tag{19}$$

From Eq. (19), we can see that φ_2 can be extracted. As a result, the two DROs can be synchronized to the MLL. However, it should be noted that only when one microwave is synchronized to the MLL can another one be synchronized, which means the two microwaves cannot be synchronized independently.

B. Impact of amplitude and phase imbalances of the RF driven signal of the DP-DMZM

To guarantee that the sub-DMZMs operate at phase modulation conditions, the two driven microwaves applied to the two RF input ports of each sub-DMZM should have the same phases and amplitudes. However, during the practical experimental operation, phase and amplitude imbalances would be introduced by the power divider, the insertion loss of each RF, and so on. The imbalances would affect the phase detection accuracy and sensitivity of the MPPD, which would further influence the residual phase noise of the MPPD. Therefore, it is necessary to explore the impact of the phase and amplitude imbalances of the microwaves on the performance of the MPPD.

To simplify the analysis, only microwave with frequency f_1 is taken into consideration. The microwave is split into two paths by a power divider, which can be expressed as $a_{11}\sin(2\pi f_1 t+\varphi_1)$ and $a_{12}\sin(2\pi f_1 t+\varphi_1+\delta\varphi)$, where a_{11} and a_{12} are the amplitudes of signals, and $\delta\varphi$ is the phase offset between the two signals. The signals at the output ports of the Sagnac loop can be written as,

$$\begin{cases} E_{\mathrm{co}x1} \propto E_{\mathrm{pulse}}(t)\left(e^{j\beta_{1+}\sin\varphi_1} + e^{j\beta'_{1+}\sin(\varphi_1+\delta\varphi)}\right) \\ E_{\mathrm{counter}1} \propto \alpha E_{\mathrm{pulse}}(t)e^{j\frac{4\pi}{3}}\left(e^{j\beta_{1-}\sin\varphi_1} + e^{j\beta'_{1-}\sin(\varphi_1+\delta\varphi)}\right) \\ E_{\mathrm{co}x2} \propto E_{\mathrm{pulse}}(t)e^{-j\frac{2\pi}{3}}\left(e^{j\beta_{1+}\sin\varphi_1} + e^{j\beta'_{1+}\sin(\varphi_1+\delta\varphi)}\right) \\ E_{\mathrm{counter}2} \propto \alpha E_{\mathrm{pulse}}(t)\left(e^{j\beta_{1-}\sin\varphi_1} + e^{j\beta'_{1-}\sin(\varphi_1+\delta\varphi)}\right) \end{cases} \tag{20}$$

Different amplitudes cause different modulation depths, which are denoted as β_{i+}, β'_{i+}, β_{i-}, and β'_{i-} (i = 1, 2), respectively in Eq. (20). According to Eq. (20), simulation is carried out to observe the influences of the phase and amplitude imbalances. Assuming that the largest output voltage of the MPPD is $V_{\max}$ and the output is $V_{\varphi 1}$ when at a fixed phase of φ_1 without phase or amplitude imbalances, while these two values are $V'_{\max}$ and $V'_{\varphi 1}$ when there exist phase or amplitude imbalances, it is obvious that the ratio between $V'_{\max}$ and $V_{\max}$ can represent the normalized detection sensitivity change. In addition, a

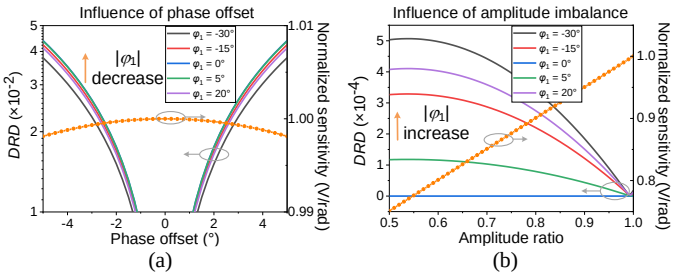

Fig. 9. (a) The error variation following the phase difference when the amplitudes are equal, $\beta_{1+}=\beta'_{1+}$, $\beta_{1-}=\beta'_{1}$. (b) The error variation following the amplitude difference when the phases are equal, $\delta\varphi=0$.

detection-ratio-difference (*DRD*) is defined as below to represent the detection accuracy error,

$$DRD = \left| \frac{V'_{\varphi_1}}{V'_{\max}} - \frac{V_{\varphi_1}}{V_{\max}} \right| \tag{21}$$

Several fixed points of φ_1 (φ_1{-30°, -15°, 0°, 5°, 20°}) are chosen to show the impact of the phase and amplitude imbalance.

Fig. 9(a) displays the variation of *DRD* with $\delta\varphi$ varying from -5° to 5° when modulation indices satisfy $\beta_{1+}=\beta'_{1+}$, $\beta_{1-}=\beta'_{1-}$, namely $a_{11}=a_{12}$. It is observed that *DRD* increases as the absolute value of φ_1 decreases when $\delta\varphi$ remains unchanged. For the same φ_1, the ratio becomes higher as $\delta\varphi$ becomes larger. This indicates that the detection result is more sensitive to the phase imbalance when the phase of the microwave approaches the pulse phase. But the *DRD* remains at a low level. The orange curve shows the normalized detection sensitivity change following the phase offset change. It is seen the detection sensitivity decreases slightly as $\delta\varphi$ deviates from zero.

Then, the case of $a_{11}\neq a_{12}$ and $\delta\varphi=0$ is considered, and the simulation results are plotted in Fig. 9(b). The *DRD* changes at two orders of magnitude lower than that when only phase offset exists. However, the detection sensitivity decreases obviously as the amplitude becomes more imbalanced.

Comparing the simulation results, we can find that the phase offset affects the detection accuracy more than the amplitude imbalance does, while the amplitude imbalance affects the detection sensitivity more than the phase imbalance does. However, both nonideal conditions show minute degradation to the system. Therefore, the system is not that sensitive to amplitude and phase imbalances.

V. Conclusion

In conclusion, we propose and demonstrate a multiplexed MPPD synchronizing two microwaves for the first time. Two microwaves with frequencies of 8.0320 GHz and 8.3332 GHz are locked to an MLL with a repetition rate of 100.4 MHz simultaneously. At the 10-kHz offset frequency, the phase noise of the 8.0320-GHz (8.3332-GHz) signal is reduced by more than 40 dB (35 dB). The integrated residual timing jitters of the two locked microwaves are 2.12 fs and 5.93 fs, respectively, indicating that they are locked at the same level. The proposed MPPD can find potential applications in distributed systems, phased-array radars, or measurement instruments.

References

[1]. A. Oz and K. Peker, "Synchronizing sample clocks of a data converter array," Analog Devices, *Inc., Tech. Rep.*.

[2]. S. L. Pan and Y. M. Zhang, "Microwave Photonic Radars", *J. Lightw. Technol.*, vol. 38, no. 19, pp. 5450-5484, Oct. 2020.

[3]. R. Quan, H. Hong, W. Xue, H. Quan, W. Zhao, X. Xiang, Y. Liu, M. Cao, T. Liu, S. Zhang, and R. Dong, "Implementation of field two-way quantum synchronization of distant clocks across a 7 km deployed fiber link," *Opt. Express*, vol. 30, no. 7, pp. 10269–10279, Mar. 2022.

[4]. Y. Chen, J. Gong, R. B. Staszewski, and M. Babaie, "A Fractional-N Digitally Intensive PLL Achieving 428-fs Jitter and <−54-dBc Spurs Under 50-mVpp Supply Ripple," *IEEE J. Solid-State Circuits*, vol. 57, no. 6, pp. 1749–1764, Jun. 2022.

[5]. J.-H. Seol, K. Choo, D. Blaauw, D. Sylvester, and T. Jang, "Reference oversampling PLL achieving –256-dB FoM and –78-dBc reference spur," *IEEE J. Solid-State Circuits*, vol. 56, no. 10, pp. 2993–3007, Oct. 2021.

[6]. T. K. Kim et al., "Sub-100-as timing jitter optical pulse trains from mode-locked Er-fiber lasers," *Opt. Lett.*, vol. 36, no. 22, p. 4443, Nov. 2011

[7]. N. Kuse, J. Jiang, C.-C. Lee, T. R. Schibli, and M. E. Fermann, "All polarization-maintaining Er fiber-based optical frequency combs with nonlinear amplifying loop mirror," *Opt. Express*, vol. 24, no. 3, pp. 3095–3102, Feb. 2016.

[8]. D. Kwon, C. Jeon, D. Kim, et al. "Femtosecond synchronization of multiple mode-locked lasers and a microwave oscillator by multicolor electro-optic sampling," *Opt. Lett.*, vol. 45, no. 11, pp. 3155-3158, Jun. 2020.

[9]. J. Kim, F. X. Kartner, and M. H. Perrott, "Femtosecond synchronization of radio frequency signals with optical pulse trains," *Opt. Lett.*, vol. 29, no. 17, pp. 2076–2078, Sep. 2004.

[10]. T. Yu, J. Fang, Q. Hao, K. Yang, M. Yan, K. Huang, and H. Zeng, "High-precision passive stabilization of repetition rate for a mode-locked fiber laser based on optical pulse injection," *Opt. Express*, vol. 29, no. 13, pp. 20930–20940, Jun. 2022.

[11]. M. Xin, et al., "Attosecond precision multi-kilometer laser-microwave network," *Light Sci. Appl.*, vol. 6, Jan. 2017.

[12]. K. Jung, et al., "Frequency comb-based microwave transfer over fiber with 7×10^{-19} instability using fiber-loop optical-microwave phase detectors," *Opt. Lett.*, vol. 39, pp. 1577–1580, Mar. 2014.

[13]. J. Kim, J. A. Cox, J. Chen, and F. X. Kärtner, "Drift-free femtosecond timing synchronization of remote optical and microwave sources," *Nature Photon.*, vol. 2, no. 12, pp. 733–736, Dec. 2008.

[14]. K. Jung, and J. Kim, "Subfemtosecond synchronization of microwave oscillators with mode-locked Er-fiber lasers," *Opt. Lett.*, vol. 37, no. 14, pp. 2958–2960, Jul. 2012.

[15]. C. Jeon, Y. Na, B. Lee, and J. Kim, "Simple-structured, subfemtosecond-resolution optical-microwave phase detector," *Opt. Lett.*, vol. 43, no. 16, pp. 3997–4000, Aug. 2018.

[16]. A. H. Nejadmalayeri, F. Kärtner "Mach-Zehnder based balanced optical microwave phase detector," *in Proc. Conf. Lasers Electro-Opt. (CLEO)*, San Jose, CA, USA, 2012, CTu2A.1.

[17]. M. Bahmanian, J. C. Scheytt, "A 2–20-GHz ultralow phase noise signal source using a microwave oscillator locked to a mode-locked laser," *IEEE Trans. Microw. Theory Techn.*, vol. 69, no. 3, pp. 1635-1645, Mar. 2021.

[18]. J. Wei, S. Zhang, J. Kim, and S. Pan, "Compact phase detector for optical-microwave synchronization using polarization modulation," *J. Lightw. Technol.*, vol. 36, no. 19, pp. 4267–4272, Oct. 2018.

[19]. K. Shao, S. Liu, P. Gao, et al. "A microwave photonic phase detector based on a dual-polarization dual-drive Mach-Zehnder modulator," in *Proc. 26th OptoElec. and Commun. Conf. (OECC)*, Hong Kong, China, 2021, M3E. 3.

[20]. X. Zhu, Z. Zheng, C. Zhang, L. Zhu, Z. Tao, and Z. Chen, "Coherent detection-based automatic bias control of Mach-Zehnder modulators for various modulation formats," *J. Lightw. Technol.*, vol. 32, no. 14, pp. 2502–2509, Jul. 2014.

[21]. M. Hyun, C. G. Jeon, and J. Kim, "Ultralow-noise microwave extraction from optical frequency combs using photocurrent pulse shaping with balanced photodetection," *Sci. Rep.*, vol. 11, no. 17809, Sep. 2021.

[22]. C. Ahn, Y. Na, M. Hyun, J. Bae, and J. Kim, "Synchronization of an optical frequency comb and a microwave oscillator with 53 zs/Hz1/2 resolution and 10-20-level stability," *Photon. Res.*, vol. 10, no. 2, pp. 365–372, Feb. 2022.